Case Studies in Construction Materials 18 (2023) e01723

Contents lists available at ScienceDirect

Case Studies in Construction Materials

journal homepage: www.elsevier.com/locate/cscm

Elastic modulus of self-compacting fibre reinforced concrete: Experimental approach and multi-scale simulation

Abdullah Alshahrani [a,b], Sivakumar Kulasegaram [a,*], Abhishek Kundu [a]

[a] School of Engineering, Cardiff University, Cardiff, UK
[b] Civil Engineering Department, College of Engineering, Najran University, Najran, Saudi Arabia

ARTICLE INFO

Keywords:
Self compacting fibre reinforced concrete (SCFRC)
Multi-scale simulation
X-ray computed tomography
Elastic modulus
Homogenisation

ABSTRACT

Evaluation of the elastic properties of self-compacting fibre-reinforced concrete is one of the primary concerns in civil and structural engineering. This paper investigates the elastic properties of self-compacting fibre-reinforced concrete with varying coarse aggregate and steel fibre content. Traditionally, the elastic properties of concrete are measured experimentally which incurs significant cost and time overhead. In this paper, a two-step homogenisation approach is proposed for predicting the elastic properties of self-compacting fibre-reinforced concrete. In the first step, the mortar, air voids and aggregates are homogenised based on mean-field homogenisation using the Mori-Tanaka model. X-ray computed tomography (CT) scanning technique was employed to analyse and determine the volume fractions, shapes, numbers of pores for validation purposes. In the second step, a finite element model of representative volume elements is generated with steel fibre inclusions and homogenised concrete to determine the overall macroscale elastic modulus of SCFRC. The results show that the content of aggregates, steel fibres and porosity in the mix has a substantial effect on the elastic modulus. The influence of fibre orientation on the elastic modulus SCFRC is also investigated. The results obtained from the homogenisation method were compared with those obtained from an experimental study and it was found that the maximum error in the elastic modulus prediction using the proposed multiscale homogenisation approach was less than 4%. This agreement between multiscale homogenisation results and experimental data highlights the feasibility of using the two-step homogenisation approach in the development of SCFRC. It has been demonstrated that the proposed homogenisation method can efficiently replace time-consuming laboratory tests, saving both resources and time.

1. Introduction

Self-Compacting Concrete (SCC) is one of the significant achievements in the construction industries within the last two decades due to its excellent rheological properties [1]. SCC is a highly flowable and non-segregating concrete that does not require vibration for its placing and compaction. It can flow due to its own weight and can flow around obstacles to fill in spaces within the formwork [2]. SCC presents many benefits over conventional concrete (CC). This includes elimination of costs and safety issues associated with concrete vibration, reduction in the construction time, and enhanced quality and durability. SCC mixes are typically designed with less content of coarse aggregates, high content of cementitious material, and a smaller maximum coarse aggregate size to achieve the

* Corresponding author.
E-mail address: kulasegarams@cardiff.ac.uk (S. Kulasegaram).

https://doi.org/10.1016/j.cscm.2022.e01723
Received 11 September 2022; Received in revised form 6 November 2022; Accepted 29 November 2022
Available online 30 November 2022

standard flow and passing ability criteria of SCC.

Numerous studies have indicated that the addition of fibre into SCC enhances many of its mechanical characteristics [3–6]. Self-compacting fibre reinforced concrete (SCFRC) combines the advantages of the SCC technology with the benefits of adding fibres to a brittle cementitious composite. On the other hand, the rheological properties of self-compacting fibre reinforced concrete (SCFRC) are significantly impaired due to the large surface area and elongated shape of steel fibres [7]. The content of fibres in SCFRC mix is limited and depends on the characteristics of the fibres and the composition of SCC. A crucial factor in the design of the SCFRC is the sand-to-aggregate (S/A) ratio, which plays an essential role in governing the fresh and hardened properties of SCFRC. Yardimici el at. [8] investigated the effect of fibre content and aspect ratio on the fresh and mechanical properties of SCFRC using different S/A ratios. Results demonstrated that when the fibre volume fraction and aspect ratio are relatively high, a higher S/A ratio should be used, which decreases the content of aggregate inversely, to enhance the flowability and fracture energy of SCFRC. These variations in the composition raise concerns as to its mechanical behaviour including the elastic properties of SCFRC. Understanding of optimum mix constituents and their effect on the mechanical performance of SCFRC is a vital area of research and development for the construction industry due to a lack of competency available in the mix design procedures [9].

Evaluating the elastic properties of concrete is of prime importance in civil and structural engineering. This becomes even more relevant when dealing with non-standard concrete such as SCC [10,11]. In the design and assessment of concrete structures, the elastic modulus of concrete is a critical mechanical parameter. It is important for ensuring the serviceability of structures and for preventing excessive deformation [12]. It is also essential in determining concrete elastic shortening and creep loss in prestressed concrete as well as in the seismic analysis for drift and deformation calculations [13]. The elastic modulus of concrete is generally affected by several factors including aggregate content and types, compressive strength, and concrete unit weight [14]. The elastic modulus is usually estimated from the concrete compressive strength according to empirical equations [13,15,16]. However, these equations do not take into consideration the effect of concrete composition and the complexity of SCC while determining the elastic modulus. According to Schlumpf [17], for SCC with same compressive strength as CC, the elastic modulus of SCC was about 20% less than that of CC. Similarly, Bonen and Shah [18] reported that the elastic modulus of SCC is lower than that of CC for comparable compressive strength. This is mainly because the elastic modulus of concrete is significantly affected by the contents of the aggregate and their elastic moduli.

There are many homogenisation techniques which have been developed with the intention of evaluating the effective elastic characteristics of composite materials, whereby a homogeneous continuum is used to substitute a heterogeneous substance. Estimating the upper and lower bounds is an example of the analytical homogenisation methods, such as, Hashin and Shtrikman bounds [19] and the Voigt and Ruess bounds [20]. Eshelby's equivalent technique [21] has been extensively used as the basis for more sophisticated analytical homogenisation techniques, such as Mori– Tanaka approximation model [22] double inclusion model [23], generalised self-consistent model [24] and the self-consistent approximation model [25]. Although effective and simple to employ, these analytical models are incapable of addressing realistic geometries or size gradations.

If an analytical homogenisation technique is insufficient for complicated microstructures such as ultra-high-performance fibre reinforced concrete (UHPFRC) [26], computational homogenisation should be applied. The direct finite element (FE) analysis of a representative volume element (RVE) is one of the most used approaches for estimating effective characteristics of composites [27,28]. The finite element approach can overcome the limitation of analytical techniques, but it is computationally expensive. Homogenisation techniques need to be simple and effective. Hence, if the analytical homogenisation techniques are sufficient, the numerical and computational approaches should be avoided to reduce errors resulting from the choice of the representative volume element (RVE) size or boundary conditions [29]. In the case of concrete, a RVE needs to be roughly 3–5 times the size of the largest aggregate diameter to be statistically representative of the bulk material [30]. However, the exact size of RVE is strongly dependent on the volume fraction of inclusions. The RVE size needs to be large enough in relation to individual grain size to represent general quantities such as stress and strain, but at the same time to be small enough to avoid hiding macroscopic heterogeneity [31]. Gal and Kryvoruk [32] proposed a two-step homogenisation approach for fibre reinforced concrete (FRC) wherein spherical aggregate, and its interfacial transition zone (ITZ) layer are homogenised first through an analytical method [33], after which numerical homogenisation is applied to the mortar, the homogenised aggregate, and the fibres to estimate the effective elastic properties of FRC. However, the influence of pores, which are inherent in cementitious composites and significantly affect the hardened properties [34], received less attention in this study.

X-ray computed tomography (CT) imaging has attracted considerable attention in recent years as a highly effective technique for characterising the internal micro and mesoscale structures of various materials due to its non-destructive nature and high-resolution images to visualise the internal details of materials. Several studies have applied X-ray CT imaging to evaluate the engineering characteristics of cement-based materials such as pore spaces [35] and spatial distribution of air-voids [36]. SCC composites are exposed to high air volumes in the fresh state which directly affects the porosity of hardened state. Ponikiewski et al. used this technique for the determination of 3D porosity of SCFRC [37].

At present, SCFRC is a widely used material in structural and civil engineering applications such as bridges, skyscrapers, tunnel linings, slabs, and other precast concrete structures [38]. However, the use of SCFRC is always accompanied by many experimental tests in the fresh and hardened state in order to meet the specifications of design standards and codes. The composition variations of SCFRC raise uncertainties with respect to its elastic properties due to a lack of competency in the mix proportioning method. A new strategy in the design and testing of SCFRC is needed to reduce experiments and cost as well as to assist with the design of mix composition and selection of its components. In this study, the elastic modulus of SCFRC designed with different content of coarse aggregates and steel fibres is investigated by experimental tests and numerical methods. Numerically, this study aims to use mesoscale finite element analysis to predict macroscopic elastic properties of SCFRC. For this, a two-step homogenisation method is proposed to evaluate the macroscopic elastic properties of SCFRC by applying Mori–Tanaka mean-field homogenisation and finite element model based computational homogenisation. As the first step, the mortar, air voids and aggregates are homogenised as plain SCC using

mean-field homogenisation. In this step, results from X-ray CT imaging technique were used to investigate the air void content of SCFRC. In the second step, a finite element model of RVE is generated with steel fibre inclusions and the homogenised SCC matrix to determine the bulk elastic modulus of SCFRC using computational homogenisation.

This paper is organised as follows. Section 2 details experimental procedures carried out to evaluate the elastic properties of SCFRC. This is followed by Section 3 which describes homogenisation methodology proposed for estimating these properties of SCFRC via computational techniques. Results of the simulation and experimental observations are summarised and compared in Section 4. In Section 5, concluding remarks are presented based on the findings.

2. Experimental programme

2.1. Raw materials and mix design

Portland cement with a specific gravity of 3.15 (from Tarmac Cement Ltd) and ground granulated blast furnace slag (GGBS) with a specific gravity of2.4 (Hanson Heidelberg Cement group) were used. Table 1 shows the chemical composition of cement and GGBS. A superplasticiser (SP) (Master Glenium ACE 499) with a specific gravity of 1.07 was used. The coarse aggregate (CA) was crushed limestone with a specific gravity of 2.65and a maximum size of 10*mm*. The fine aggregate (FA) is natural river sand with a specific gravity of 2.55and a maximum size of 2mm.A part of natural river sand was replaced by an equivalent volume (30%) of the coarser fraction of limestone powder with size ranging between 0.125*mm* and 2 *mm* and a specific gravity of 2.6. The gradation of fine and coarse aggregate is given in Fig. 1. The steel fibre used is Dramix 3D 55/30 BG with hooked ends and 30 mm long and a diameter of 0.55 mm. The density, aspect ratio and tensile strength for the steel fibres used are 7800 kg/m^3, 55 and 1345 N/mm^2respectively. Four series of high strength SCC mixes were designed based on the mix design method proposed in [39,40]. The details and percentage relative proportions of the mixes are given in Tables 2 and 3, respectively. The mixes are designated according to their coarse aggregate content in case of SCC and fibre content in case of SCFRC (please refer Table 3 for more details).

2.2. Specimen preparation and test procedure

Slump flow test and J-ring test were conducted according to ENFARC [41] to ensure that all mixes satisfied the flow and passing ability criteria without any sign of segregation. According to the mix proportions of high strength SCC, three cubes $(100mm)$, cylinders $(100 \times 200mm)$ for each group were cast. In order to investigate the volume of air voids, a beam of $(150 \times 150 \times 600mm)$were also cast. A cube of $(100 \times 100 \times 100mm)$ size was cut from the central part of the beam to be used for X-ray CT imaging for investigating the porosity of the mix. This is an important step as SCFRC composite are prone to contain significant amount of air voids in the fresh state compared to CC. The specimens were then de-moulded after 1 day and cured in water at a temperature of $20(\pm 2)^{\circ}C$ for 28 days. The compressive strength test was performed according to the method proposed in [42]. The modulus of elasticity $(E)$was measured according to the method recommended in [43] by slowly loading a cylindrical sample until it reached about a third of its failure load and then measuring the resulting strain. 30 mm strain gauge was used to measure the strain. Experimental setup and diagram for testing the elastic modulus under static loading is shown in Fig. 2. Three loading cycles were carried out for each specimen from (0.5MPa) to one third of the compressive strength with a loading rate of 0.5 MPa/s to calculate the modulus of elasticity.

The modulus of elasticity (E) was calculated using Eq. (1).

$$E = \frac{\Delta\sigma}{\Delta\varepsilon_s} \tag{1}$$

where, E is the modulus of elasticity (in MPa), $\Delta\sigma$ is the difference stress between preloading stress (0.5MPa) and upper loading stress (one-third of the compressive strength). $\Delta\varepsilon_s$is the strain difference during third loading cycle.

2.3. X-ray computed tomography (CT) scanning

X-ray (CT) scanning is an effective non-destructive technique for acquiring a large number of successive 2D slice images of the internal microstructure of samples. In this study, it was used to analyse the volume, distribution, shapes, and numbers of large pores within the SCFRC. The CT equipment used was the General Electric GE CT scan. The total number of CT slices image was 882 with a slice thickness of 0.27*mm*. The voltage and current of X-ray tube settings for the scan were 140kV and 180μA, respectively.

Table 1
The chemical composition of cement and GGBS.

Composition	SiO_2	Al_2O_3	Fe_2O_3	CaO	K_2O	Na_2O	MgO	So_3	TiO_2
Cement (%)	19.69	4.32	2.85	63.04	0.74	0.16	2.17	3.12	0.33
GGBS (%)	34.34	12.25	0.32	39.90	0.45	0.41	7.70	0.23	0.65

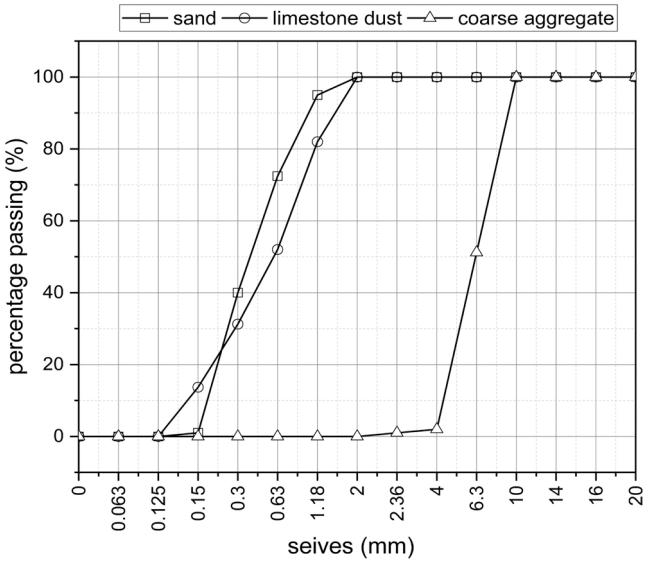

Fig. 1. The gradation of fine and coarse aggregate.

Table 2
Mix proportions of SCC mixes, (kg/m^3).

Mix designation	Water	Cement	GGBS	SP	FA	CA	Fibre
SCC-20	205.6	308.4	205.6	2.6	997.5	530	–
SCFRC-1	205.6	308.4	205.6	3.6	972	530	78
SCC-30	205.6	308.4	205.6	2.3	739	796	–
SCFRC-0.5	205.6	308.4	205.6	3	726	796	39

Table 3
Percentage and relative proportions of mixes.

Cementitious material - OPC + 40% GGBS			Water to cement ratio (w/cm) = 0.40	
Mix designation	Content of coarse aggregate		Content of mortar	Percentage of steel fibre
	By volume			
SCC-20	0.2	0.8		0
SCFRC-1	0.2	0.79		1
SCC-30	0.30	0.70		0
SCFRC-0.5	0.30	0.695		0.5

3. Homogenisation methodology

The local homogenisation of macroscopic solids is commonly utilised in the multi-scale method to address mechanical characteristics at the meso-scale [32,44,45]. The link between macro-scale and mesoscale is created through a statistically representative model (RVE) of the microstructure. The RVE is composed of inhomogeneous materials consisting of a wide range of geometric and mechanical properties in the mesoscale level. The macroscopic mechanical behaviour of RVE is predicted via continuum mechanics to determine the macroscopic constitutive response of the composite by using the constitutive behaviour of each phase. At the macro scale, each material point is assumed to be the centre of the RVE, which needs to be adequately large to accurately describe the underlying inhomogeneous microstructure, and simultaneously small enough in comparison to the size of the solid body. Fig. 3 depicts a schematic diagram of two-step homogenisation process.

This paper proposes a novel two-step homogenisation method for investigating the elastic properties of SCFRC, from the mesoscale level. The first step for evaluating the elastic properties of SCC is by mean-field homogenisation (MFH) using Mori-Tanaka model. At this stage, mortar is equivalent to the homogeneous body and considered as the matrix while the CA and pores are treated as inclusions. In the second step, computational homogenisation is performed for the homogenised concrete (which include CA and pores) from step 1 (as matrix) and steel fibres (as inclusions). The developed approach hence combines the efficient semi-analytical method and the numerical simulation procedure. This method can predict the elastic modulus of SCFRC based on its compositions wherein the effect of both fibre orientation and pore distribution are simultaneously considered.

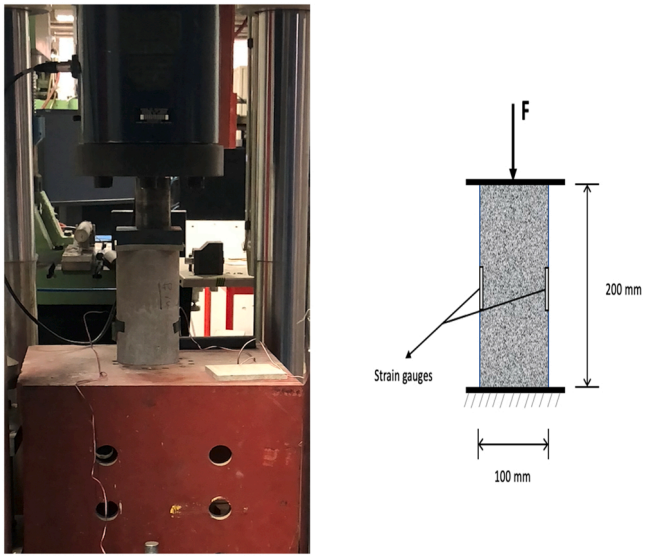

Fig. 2. Modulus of elasticity test: experimental set-up (right) and specimen dimensions (left).

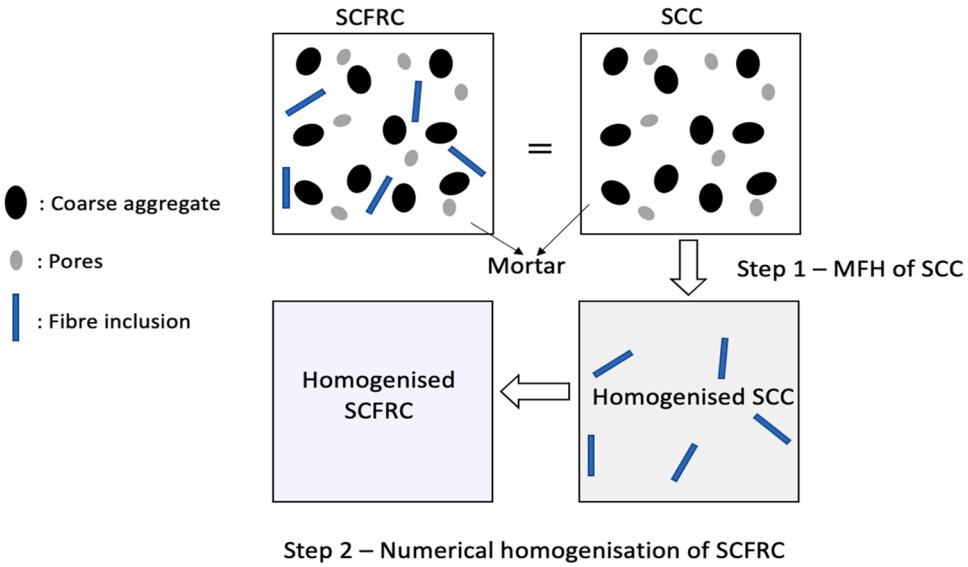

Fig. 3. Schematic of the two-step homogenisation process.

3.1. Step-1 – mean-field homogenisation (MFH)

Based on a set of assumptions, several homogenisation models have been developed by adopting Eshelby single inclusion theory [21] including the generalised self-consistent model [24], the Mori–Tanaka approximation model [22], and the double inclusion model [23]. The macroscopic properties of composite materials are deduced based on the volume proportion of inclusions, the shape of the inclusions and the properties of the constituent materials. Among these models, the Mori–Tanaka model [22] is widely used for the prediction of effective characteristics of composite materials. The original Mori-Tanaka model for composites with only one type of inclusions was extended by Benveniste [46] by generalising the model for RVEs with several inclusions of similar shape. The details of the Mori– Tanaka model [22,46] can be found in [47]. The mean-field homogenisation schemes work by relating the mean stress and strain in the RVE. The mean of the stress/strain field, f, over RVE of domain $\omega$with a volume υ is given as follow:

$$\langle f \rangle = \frac{1}{\upsilon}\int_{\omega} f(x,\bar{x})d\upsilon, \tag{2}$$

In the above equation, f is the internal stress/strain field, $\bar{x}$is the macro point, x is the meso point. Where the integration is

performed with respect to meso-coordinates x in the RVEω..

The mean of the stress/strain field over a single phase is given by:

$$\langle f \rangle_{\omega_i} = \frac{1}{v_i}\int_{\omega_i} f(x,\bar{x})dv_i, \mathrm{i} = 0, 1 \tag{3}$$

In Eq. (3), 0 represents the matrix while 1 represents the inclusion.

The relationship between the average strains of RVE, the matrix, and the inclusion is given by Eq. (4), whereas Eq. (5) shows the average stress relationship.

$$\langle \varepsilon \rangle_{\omega} = \nu_o \langle \varepsilon \rangle_{\omega_0} + \nu_1 \langle \varepsilon \rangle_{\omega_1} \tag{4}$$

$$\langle \sigma \rangle_{\omega} = \nu_o \langle \sigma \rangle_{\omega_0} + \nu_1 \langle \sigma \rangle_{\omega_1} \tag{5}$$

where ν_0 and ν_1 are the volume of matrix and inclusion, respectively, and $\nu_0 + \nu_1 = 1$.

The strain fields within different phases and the whole RVE are related to each through the so-called strain concentration tensors (A and B) such that

$$\langle \varepsilon \rangle_{\omega 1} = B^{\varepsilon} : \langle \varepsilon \rangle_{\omega_0}; \langle \varepsilon \rangle_{\omega 1} = A^{\varepsilon} : \langle \varepsilon \rangle_{\omega} \tag{6}$$

The volume average of strain over all inclusions are connected to the volume average of strain over the matrix phase through the first tensor. On the other hand, the second tensor relates the average volume strain over the entire RVE (macro strain) to the average volume strain over all inclusions. The two strain concentration tensors are dependent, as the latter one can be determined from the former

$$A^{\varepsilon} = B^{\varepsilon} : [\nu_1 B^{\varepsilon} + (1 - \nu_1)\boldsymbol{I}]^{-1} \tag{7}$$

where $\boldsymbol{I}$ represent the symmetric equivalent tensor, changing with B^{ε}.

Sophisticated MFH models are based on the fundamental solution of Eshelby. The problem of a single ellipsoidal inclusion (I) of uniform stiffness C_1,which is embedded in an infinite matrix of uniform stiffness C_0 can be solved by using Eshelby's solution. It is found that the strain inside the inclusion is uniform and related to the remote strain under a remote uniform strain (E) by,

$$\varepsilon(x) = H^{\varepsilon}(I, C_1, C_0) : E, \forall \in (I) \tag{8}$$

where H^{ε} is the single inclusion strain concentration tensor.

The macro stiffness for any homogenisation model specified by a strain concentration tensor is;

$$C = [\nu_1 C_1 : B^{\varepsilon} + (1 - \nu_1)C_0] : [\nu_1 B^{\varepsilon} + (1 - \nu_1)\boldsymbol{I}]^{-1} \tag{9}$$

where the subscript 0 represents the matrix and 1 represents inclusions.

In the macro-scale, the relationship between stress and strain is given by

$$\overline{\sigma} = \overline{C} : \overline{\varepsilon} \tag{10}$$

In this study, the homogenisation of SCFRC starts with the homogenisation of CA and the pores. The elastic properties of SCC are predicted using mean-field homogenisation Mori-Tanaka model. Li et al. [48] suggested an image-processing based method for evaluating the aspect ratio of CA and found that the median aspect ratio value to be 1.33. The volume fraction of the air voids was 0.1% and the shape of pores was assumed to be spherical which is supported by the experimental observations of CT scanning (see Fig. 5). Table 4 presents the mechanical property parameters of each phase of SCFRC. The elastic modulus and Poisson's ratios of aggregate were acquired from [49], while the densities of aggregate, mortar, as well as the elastic modulus of mortar, were measured experimentally in the laboratory. The prediction of the elastic properties of SCC was implemented in the Digimat-MF which is a powerful tool for calculating material characteristics that incorporates Mori-Tanaka homogenisation. Mori-Tanaka model can ensure rapid calculation of heterogeneous material characteristics and is extremely computationally efficient.

Table 4
Mechanical properties of high strength SCC components.

	Phase	Elastic modulus (GPa)	Poisson's ratio μ	Density (kg/m^3)
Step 1	Mortar	31.1	0.2	2250
	Aggregate	74.5	0.2	2650
	Porosity	–	–	–
Step 2	Homogenised concrete			
	1. SCC-20	36.60	0.2	2330
	2. SCC-30	39.77	0.2	2370
	Steel fibre	200	0.3	7800

3.2. Step-2 – finite element method based numerical homogenisation

Numerical homogenisation, which typically uses the finite element (FE) method to represent sophisticated heterogeneous material structures at varying length scales, is an alternative to analytical technique. The computational homogenisation technique [26,50] is adopted here to predict the effective elastic characteristics of SCFRC. In this study, the evaluation of elastic properties of SCFRC was performed based on two-step homogenisation method. After determining the homogenised properties of SCC using mean-field homogenisation process, the homogenised plain SCC with embedded steel fibres was simulated using finite element models based on RVEs of the composite assuming homogenised SCC as the matrix and steel fibres as inclusions. The fundamental constitutive relation of a heterogeneous material can be defined as follows in terms of computational homogenisation:

$$\langle \sigma \rangle = \overline{C} : \langle \varepsilon \rangle \tag{11}$$

In order to extract the equivalent orthotropic properties of SCFRC, six independent loadings with periodic boundary condition are performed on (RVEs) which is denoted as "automatic properties evaluation" in Digimat-FE. These six loadings are tensile load in 11 directions, tensile load in 22 direction, tensile load in 33 directions, shear load in 12 directions, shear load in 23 directions and shear load in 13 directions. For this purpose, RVE generation algorithms available in Digimat-FE were used to generate random 3D geometric models of the meso-structural features based on the geometric shape and volume fraction of steel fibre. The mechanical properties of the steel fibre and all phases are given in Table 4.

4. Results and analysis

4.1. Experimental results

The results obtained for slump flow test and J-ring test are given in Table 5. All tested mixes had shown no signs of bleeding or segregation during thorough visual inspections. The results of the compressive strength, unit weight and elastic modulus of the specimens are shown in Table 6. It is well known that the compressive strength of SCC and SCFRC is dominantly controlled by the water to cementitious materials ratio. However, the results show the elastic modulus of SCC significantly increases with the addition of CA for the same compressive strength. For example, the mix with 30% of CA by volume (i.e., SCC-30) yielded an elastic modulus (E_{exp}) of 41.06(GPa)while SCC-20 produced 37.02(GPa)while both mixes achieved approximately same target compressive strength of 70 MPa. This clearly demonstrates the limitation of the empirical equations that estimated the elastic modulus from the compressive strength and neglected the effect of SCC and SCFRC mix composition on the evaluation elastic modulus. Also, it can be observed that the addition of steel fibre further enhances the elastic modulus of SCFRC.

Several relationships have been suggested for the prediction of the elastic modulus of concrete, mainly from the compressive strength of concrete, but these models may predict the elastic modulus of SCC inaccurately due to the lower content of aggregate [13]. The elastic modulus of concrete depends on the proportion of the individual constituents and their Young's moduli. Hence, the elastic modulus of concrete improves with increasing volume fraction of CA, while it reduces when the content of mortar and porosity increases [11]. The assessment of the elastic properties of SCFRC is often conducted through experimental tests, whereas the use of computational modelling is very limited. In this study, multi-scale numerical simulation of SCFRC is proposed for the prediction of effective elastic properties.

4.1.1. X-ray computed tomography (CT) results

The main purpose of harnessing the X-ray CT is to determine the volume fraction of the large of pores and the number of large pore size the inside the concrete. From the CT images, the identification of different materials is based on the density of each material. The greyscale of CT scans of material will increase as the density of the material increases. Steel fibres have the highest density among all the constituent materials in SCFRC, hence steel fibres have the maximum greyscale and represent the brightest colours in CT images. Fig. 4 shows one of the CT image series, in which steel fibres, CA, voids and mortar can be seen and distinguished from each other.

The digital images produced by the CT scanner were analysed using the MIMICS image-processing software, which is a powerful tool in the reconstruction of CT images data [51]. Image segmentation, which is a process of detecting objects or the region of interest (ROI) from an input image, is an important stage in the transition from image processing to image reconstruction and analysis. Thresholding is a simple and efficient approach for image segmentation in digital image processing among several image segmentation methods [52]. MIMICS image-processing software was used to segment the 3D image into multiple phases based on greyscale

Table 5
Slump flow test and J-ring flow test of SCC mixes.

Mix designation	Slump flow test		J-ring[a] flow test	
	Spread (mm)	t_{500} (s)	Spread (mm)	t_{500j} (s)
SCC-20	690	1.8	680	2.1
SCFRC-1	730	1.5	670	2.2
SCC-30	740	1.7	680	2
SCFRC-0.5	770	2	690	2.3

[a] J-ring apparatus with 12 steel rods.

Table 6
Results of compressive strength and elastic modulus for all mixes at 28 days.

Mix designation	Compressive strength (MPa)	Unit weight (kg/m^3)	Elastic Modulus (E_{exp}) (GPa)
SCC-20	71.9	2311	37.02
SCFRC-1	73.7	2361	38.55
SCC-30	71.7	2398	41.06
SCFRC-0.5	69.2	2403	41.62

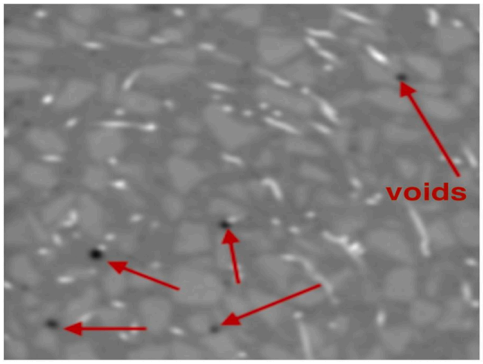

Fig. 4. 2D slice image from CT scan.

thresholds (−1024 to 3071). By filtering out image elements with greyscale levels with predefined threshold values, the images of voids can be acquired. After image thresholding segmentation, some defects may appear in the image which needs to be eliminated. The limitations of greyscale thresholds should thus be selected carefully. To identify air voids, a threshold in the range of – 1024 to –70 was adopted which is consistent with the values reported in [53].

3D configuration of the air voids is presented in Fig. 5 in which air voids volume fraction is approximately 0.1%. The total number of air voids is 298, and the frequency histogram of air voids is shown in Fig. 6. The results of this study reveal that majority of air voids in the SCFRC are characterised by a small volume (less than $1mm^3$) which is in line with previous study [37].

4.2. Numerical simulations results

4.2.1. Step 1 – mean-field homogenisation for self-compacting concrete

The prediction of effective elastic modulus of SCC was performed based on MFH using the Mori-Tanaka homogenisation technique [22,46]. The results of the elastic properties obtained for SCC mixes are given in Table 7. Though Mori-Tanaka model can provide an excellent prediction for the effective properties of materials, it is not appropriate for high volume fractions of inclusions (i.e., for more than 30%) [30]. In case of SCC, the volume fraction of inclusions (i.e., aggregates) is typically less than 30% and thus, this model can be successfully used to predict the macroscopic properties of SCC. The main advantage of using MFH method is low computational cost.

The interfacial transition zone (ITZ) between the matrix and the inclusions in SCC and UHPFRC are different from that in ordinary concrete designed with higher w/cm ratio [26,29,54,55]. Stefaniuk et al. [29] investigated the interfacial transition zone (ITZ) in SCC using X-ray micro-CT and line indentation. Results show that the ITZ in SCC is as rigid as the bulk matrix and have no significant effect

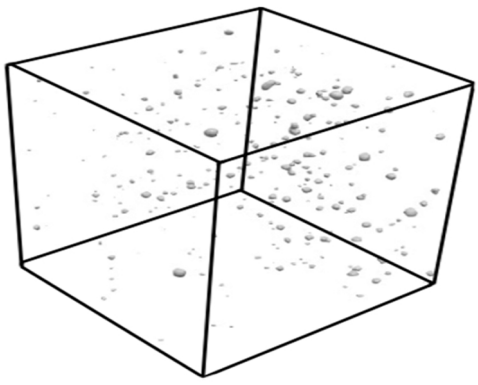

Fig. 5. 3D image reconstruction of pores.

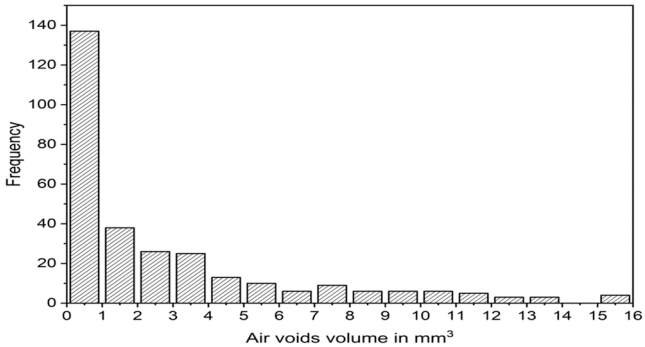

Fig. 6. Frequency distribution of air voids volume in mm^3.

Table 7
Mechanical properties of SCC obtained by mean-field homogenisation method.

Mix designation	Mori Tanaka model		Density (Kg/m^3)
	E_H (GPa)	μ_H	
SCC-20	36.60	0.2	2330
SCC-30	39.77	0.2	2370

in the SCC composites and thus was neglected in SCC homogenisation techniques in the present work. This strength in the ITZ in SCC can be related to several factors such as low water-cementitious material ratios, smaller maximum aggregate sizes, less coarse aggregate contents, and use of supplementary cementitious materials [56]. The use of GGBS can enhance the mechanical and durability properties because GGBS considerably reduces the size and content of $Ca(OH)_2$ crystals in the aggregate-paste interface, which makes the microstructure of the transition zone between aggregate and powder dense and strong [57,58].

4.2.2. Step 2 – numerical homogenisation

Several researchers have shown that introducing fibres into self-compacting concrete increased the efficiency of achieving uniform dispersion of fibres within structural components due to the rheological stability of the SCC matrix [6,49]. The properties of SCFRC are significantly dependent on the fibre content, fibre orientation, the fibre aspect ratio, and the properties of SCC matrix itself [3]. The fibre orientation in SCC is influenced by several factors: rheological properties, formwork geometry, fibre geometry, casting parameters into the formwork, wall effect, etc. [59]. In general, the steel fibre reinforced concrete is regarded as isotropic materials and the steel fibres are assumed to be randomly distributed in the concrete [60].

In the second step of the proposed homogenisation method, the inclusions i.e., fibres were modelled as cylinders with a length of $30mm$ and a diameter of $0.55mm$ giving them an aspect ratio of 55. The inclusions were randomly distributed in the matrix (see Figs. 7 and 8). The first step in any RVE based numerical homogenisation is to check whether the homogenised properties are independent of the size of the RVE. Since the RVEs are computationally generated with inclusions placed randomly within the matrix material, the

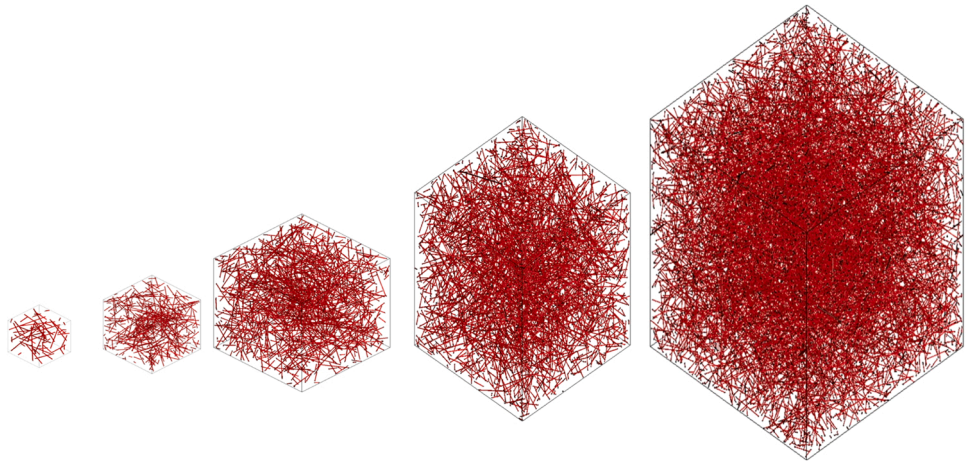

Fig. 7. Different RVE size with random orientation of fibres, from left 25 mm, 50 mm, 75 mm, 100 mm, and 150 mm.

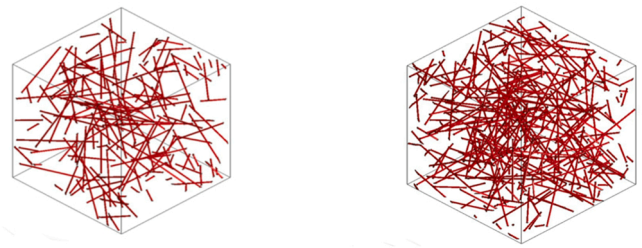

Fig. 8. Final RVEs with steel fibre volume fractions of (a) 0.5% left, and (b)1% right.

homogenised properties vary with every random realisation of the RVE giving slightly different properties. To account this, RVEs of several sizes were made (see Fig. 7). The homogenisation results are shown in Table 8. The RVE size was defined by the length of one of its edges. The number of inclusions is determined using the volume fraction of the inclusions which was set to 1%. The results of this analysis showed that for the prediction of elastic properties of SCFRC, there is no significant dependence of homogenised properties on the size of RVE exists. The variation in the homogenised RVE properties have stabilised as a function of RVE sizes within the range investigated in this study.

The RVE size selected for the proceeding analysis was $(50 \times 50 \times 50mm)$ and as per the experiments two cases (i.e., 0.5% and 1%) of volume fractions of inclusions were considered (see Fig. 8). The number of inclusions were 88 and 175 for mix SCFRC-0.5 and SCFRC-1, respectively. The meshes were generated using voxel meshes for the FE model. The number of elements and nodes were 125,000 and 132,651, respectively. The average elastic modulus predicted from the proposed method for SCFRC-0.5 are $E_{11} = 40.19GPa$, $E_{22} = 40.18GPa$ and $E_{33} = 40.19\ GPa$ while the average elastic modulus for SCFRC-1 are $37.39GPa$ for E_{11}, E_{22} and E_{33}. Hence, the average elastic modulus of SCFRC obtained from the analysis of mesoscale level using the two-step homogenisation method was $40.19GPa$ and $37.39GPa$ for SCFRC-0.5 and SCFRC-1, respectively.

4.3. Validation of proposed homogenisation method

To validate the complete two-step homogenisation methodology for determining the elastic modulus of SCFRC, the results of homogenisation were compared with the experimental results. These are shown in Table 9. The comparison clearly demonstrates that the elastic modulus predicted by multi-scale numerical simulation using the mean fields homogenisation method and finite element simulation for SCFRC is in excellent agreement with the experimental results. The consistency between the obtained numerical findings and the experimental data demonstrates the viability of using computer simulation in the design of multiphase materials. The coupling of mean-field homogenisation and finite element homogenisation, for the prediction of effective properties of SCFRC, results in enormous savings of computational efforts compared to using numerical homogenisation in both steps. The ability to predict the mechanical properties of SCFRC could be very appealing to the concrete industry as it would make it possible to deliver a more predictable products especially in the case of SCFRC as it is very difficult to predict its mechanical properties compared to CC. The method proposed in the current work can also be used for preliminary mix optimisation and the selection of constituents for SCFRC. It can be concluded that the proposed two-step homogenisation method can effectively replace time-consuming laboratory tests, saving time and the cost of raw materials. This method combines efficient MFH technique and numerical simulation to predict the elastic properties of SCFRC based on its composition while incorporating the effect pores which inherently exist in cement-based composites.

4.4. Effect of coarse aggregate and fibre volume fraction on homogenised elastic modulus

The two-step homogenisation method proposed in the current work was used to study the effect of CA and fibre volume fractions on the homogenised elastic modulus of SCFRC. The results obtained in this study are presented in Fig. 9 which shows that the model can correctly capture the improvement in the elastic modulus with increasing volume fractions of CA and fibres. The results also highlight that the effect of fibres and CA in increasing the elastic modulus. Increasing the CA volume fraction from 0% to 30% increase the elastic modulus by around $9GPa$ irrespective of the fibre volume fraction. Similarly, increasing the fibre volume fraction 0%to 2% increases the elastic modulus by around $1.6GPa$ irrespective of the CA volume fraction.

4.5. Effect of porosity and fibre orientation on the elastic modulus

As SCC are susceptible to excessive air volumes in the fresh mix which mainly affects the porosity of the concrete structure. In order to understand the effect of the volume fraction of porosity on the elastic modulus of SCC, the elastic modulus of SCC was predicted with different content of pores. Fig. 10 illustrates the effect of porosity of 0%, 0.5%, 1% and 2% on the elastic modulus of SCC. The results indicate the degree of influence of porosity volume fraction on the elastic modulus of SCC. It can be observed that the porosity has a substantial effect on the elastic modulus.

To evaluate the degree of influence of steel fibre orientation on the elastic modulus of SCFRC, an RVE corresponding to SCFRC-1 was simulated with all the steel fibres randomly distributed but their orientations are aligned along the x-axis. The results of the elastic modulus are $E_{11} = 38.12GPa$, $E_{22} = 37.16GPa$ and $E_{33} = 37.16\ GPa$. And as expected, the elastic modulus in x-direction (E_{11}) is

Table 8
Engineering constants for RVEs of different sizes.

RVE size (mm)	25	50	75	100	150
Number of fibres	22	175	592	1403	4735
E_{11} *(GPa)*	37.38	37.39	37.38	37.37	37.39
E_{22} *(GPa)*	37.40	37.39	37.37	37.37	37.39
E_{33} *(GPa)*	37.37	37.39	37.37	37.38	37.39
G_{12} *(GPa)*	0.20040	0.20022	0.20024	0.20019	0.20019
G_{23} *(GPa)*	0.20053	0.20033	0.20019	0.20020	0.20022
G_{23} *(GPa)*	0.20070	0.20020	0.20024	0.20019	0.20021
μ_{12}	0.20047	0.20026	0.20024	0.20020	0.20022
μ_{21}	0.20068	0.20026	0.20020	0.20021	0.20020
μ_{13}	0.20033	0.20020	0.20025	0.20022	0.20019
μ_{31}	15.54	15.54	15.53	15.53	15.53
μ_{23}	15.53	15.54	15.53	15.53	15.53
μ_{32}	15.53	15.53	15.53	15.53	15.53
Density (kg/m^3)	2384.7	2384.7	2384.7	2384.7	2384.7

Table 9
Comparison of experimental and homogenised elastic modulus.

Mix designation	(E_H) (GPa)	(E_{exp}) (GPa)	Discrepancy %
SCC-20	36.60	37.02	1.13
SCFRC-1%	37.39	38.55	3.01
SCC-30	39.77	41.06	3.14
SCFRC-0.5%	40.19	41.62	3.44

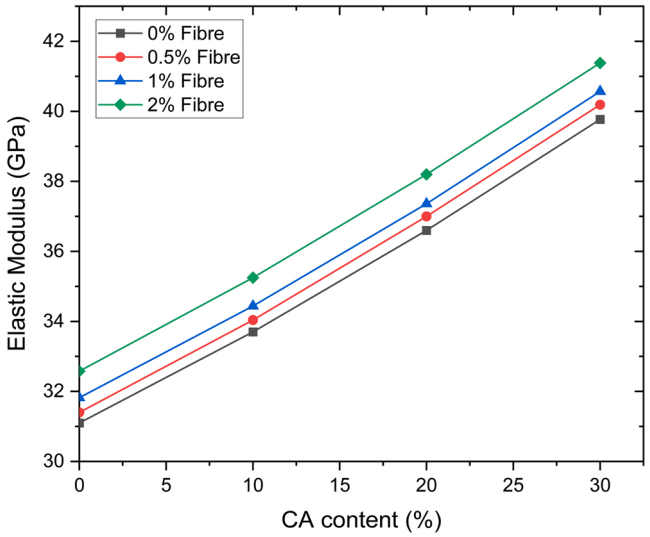

Fig. 9. Effect of CA and fibre volume fraction on homogenised elastic modulus.

estimated to have maximum value. Further, the deviation between E_{11} and E_{22} (or E_{33}) was around 0.96*GPa* whereas when the fibres were randomly oriented fibres the variation between E_{11} and E_{22} (or E_{33}) is approximately zero as noted in Table 8. For further analyses, the above exercise was repeated for RVE models with higher fibre volume fraction (e.g., 2%) where the comparison was made on elastic modulus between RVE with fibres being randomly oriented and the RVE with all fibres aligned along x-axis (see Fig. 11). In the case of all fibres are all aligned the x-axis, the averaged elastic modulus is E_{11}= 39.67*GPa*, E_{22} = 37.75*GPa* and E_{33} = 37.75 *GPa*. It can be noticed E_{11} is approximately 5% higher than E_{22} and E_{33} (around 1.92 *GPa*). While in the case where the fibres were randomly oriented, the averaged elastic modulus is E_{11}= 38.20 *GPa* , E_{22} = 38.19*GPa* and E_{33} =38.19 *GPa*. This indicates only a 0.01*GPa* difference between E_{11}, E_{22} and E_{33}. This demonstrates that the influence of fibre orientation on elastic modulus of SCFRC becomes more significant with increasing fibre volume fraction.

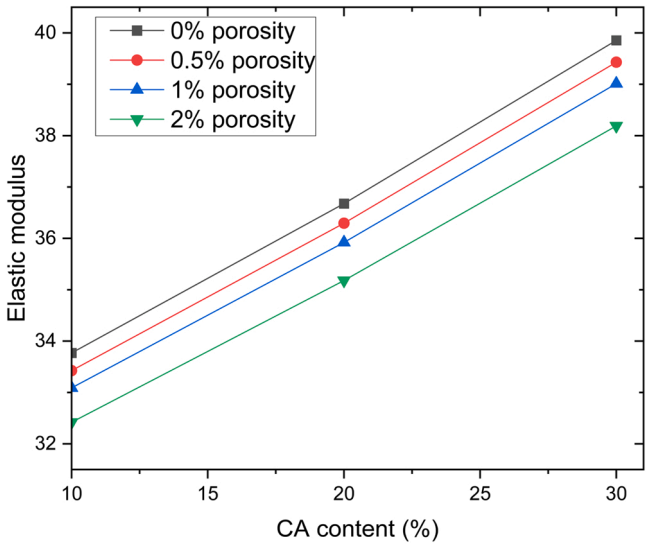

Fig. 10. Effect of the porosity on the homogenised elastic modulus.

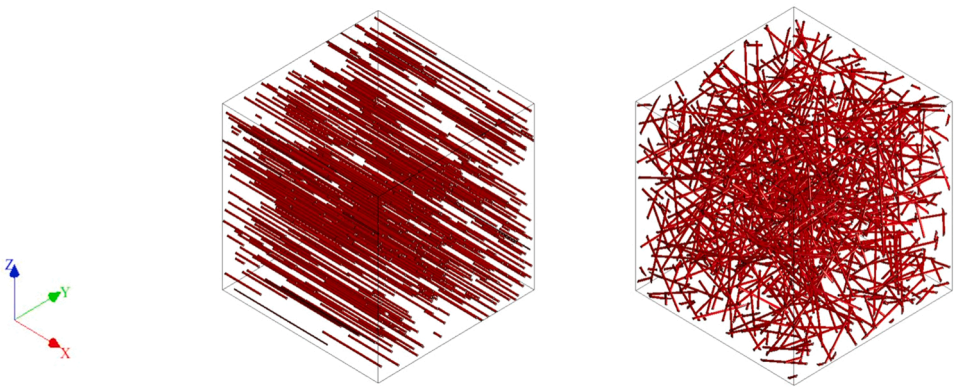

Fig. 11. RVEs with different fibre orientations (a) aligned along x-axis (left), (b) random (right).

5. Conclusion

In the current study, the elastic modulus of SCFRC was determined experimentally and using a proposed two-step homogenisation method. Experimentally, four different concrete mix compositions with the same w/cm ratio were prepared and analyzed. Although all mixes achieved approximately 70 MPa of compressive strength, the elastic modulus is influenced by the mix compositions of SCFRC. Image analysis performed on X-ray CT scans of the concrete samples showed the volume shape of pores of which is a range of sizes exist within the concrete microstructure but the majority of the pores are very small ($\leq 1\ mm^3$). The elastic modulus of SCFRC was also predicted using the two-step homogenisation method by coupling Mori–Tanaka mean-field homogenisation and finite element model-based computational homogenisation. The mortar, air voids and aggregates are homogenised as SCC using mean-field homogenisation as the first step. Numerical homogenisation is performed for the homogenised SCC and steel fibres as the second step. A comparison of the estimated elastic modulus with experimentally determined values showed that the results of the proposed method agree very well with experimental findings with a maximum error of only 3.44% in the estimated elastic modulus. The investigations and results presented in this paper are limited to predictions of elastic properties of self-compacting fibre reinforced concrete. For a comprehensive analysis of hardened state of the concrete, it is essential to introduce a nonlinear constitutive damage model in mesoscale to predict the strength and fracture properties of SCFRC. This will be one of the main objectives of our future work. Furthermore, the effect of fibre orientation and porosity on the elastic modulus SCFRC is evaluated. The proposed two-step homogenisation method can quickly and effectively replace time-consuming laboratory testing, saving time and resources on raw materials. It can also be employed for initial mix optimisation and the selection of constituents of SCFRC.

Declaration of Competing Interest

The authors declare that they have no known competing financial interests or personal relationships that could have appeared to influence the work reported in this paper.

Data availability

Data will be made available on request.

References

[1] P. Dinakar, S.N. Manu, Concrete mix design for high strength self-compacting concrete using metakaolin, Mater. Des. 60 (2014) 661–668, https://doi.org/10.1016/j.matdes.2014.03.053.
[2] H. Okamura, K. Ozawa, Self-compacting high performance concrete, Struct. Eng. Int. J. Int. Assoc. Bridge Struct. Eng. 6 (1996) 269–270, https://doi.org/10.2749/101686696780496292.
[3] R. Deeb, B.L. Karihaloo, S. Kulasegaram, Reorientation of short steel fibres during the flow of self-compacting concrete mix and determination of the fibre orientation factor, Cem. Concr. Res. 56 (2014) 112–120, https://doi.org/10.1016/j.cemconres.2013.10.002.
[4] J.H. Haido, B.A. Tayeh, S.S. Majeed, M. Karpuzcu, Effect of high temperature on the mechanical properties of basalt fibre self-compacting concrete as an overlay material, Constr. Build. Mater. 268 (2021), 121725, https://doi.org/10.1016/j.conbuildmat.2020.121725.
[5] R. Madandoust, M.M. Ranjbar, R. Ghavidel, S. Fatemeh Shahabi, Assessment of factors influencing mechanical properties of steel fiber reinforced self-compacting concrete, Mater. Des. 83 (2015) 284–294, https://doi.org/10.1016/j.matdes.2015.06.024.
[6] S.S. Majeed, J.H. Haido, D.S. Atrushi, Y. Al-Kamaki, Y.Z. Dinkha, S.T. Saadullah, B.A. Tayeh, Properties of self-compacted concrete incorporating basalt fibers: experimental study and gene expression programming (GEP) analysis, Comput. Concr. 28 (2021) 451–463, https://doi.org/10.12989/cac.2021.28.5.451.
[7] R. Deeb, A. Ghanbari, B.L. Karihaloo, Development of self-compacting high and ultra high performance concretes with and without steel fibres, Cem. Concr. Compos 34 (2012) 185–190, https://doi.org/10.1016/j.cemconcomp.2011.11.001.
[8] M.Y. Yardimci, B. Baradan, M.A. Taşdemir, Effect of fine to coarse aggregate ratio on the rheology and fracture energy of steel fibre reinforced self-compacting concretes, Sadhana Acad. Proc. Eng. Sci. 39 (2014) 1447–1469, https://doi.org/10.1007/s12046-014-0257-2.
[9] S.A. Rajakarunakaran, A.R. Lourdu, S. Muthusamy, H. Panchal, A. Jawad Alrubaie, M. Musa Jaber, M.H. Ali, I. Tlili, A. Maseleno, A. Majdi, S.H.M. Ali, Prediction of strength and analysis in self-compacting concrete using machine learning based regression techniques, Adv. Eng. Softw. 173 (2022), 103267, https://doi.org/10.1016/j.advengsoft.2022.103267.
[10] A. Vilanova, J. Fernandez-Gomez, G.A. Landsberger, Evaluation of the mechanical properties of self compacting concrete using current estimating models: estimating the modulus of elasticity, tensile strength, and modulus of rupture of self compacting concrete, Constr. Build. Mater. 25 (2011) 3417–3426, https://doi.org/10.1016/j.conbuildmat.2011.03.033.
[11] K. Holschmacher, Y. Klug, A database for the evaluation of hardened properties of SCC, Lacer 7 (2002) 123–134.
[12] F.P. Zhou, F.D. Lydon, B.I.G. Barr, Effect of coarse aggregate on elastic modulus and compressive strength of high performance concrete, Cem. Concr. Res. 25 (1995) 177–186, https://doi.org/10.1016/0008-8846(94)00125-I.
[13] F. Aslani, S. Nejadi, Mechanical properties of conventional and self-compacting concrete: an analytical study, Constr. Build. Mater. 36 (2012) 330–347, https://doi.org/10.1016/j.conbuildmat.2012.04.034.
[14] J.G. Jawahar, C. Sashidhar, I.V.R. Reddy, J.A. Peter, Effect of coarse aggregate blending on short-term mechanical properties of self compacting concrete, Mater. Des. 43 (2013) 185–194, https://doi.org/10.1016/j.matdes.2012.06.063.
[15] Eurocode 2, Design of Concrete Structures-Part 1–1: General Rules and Rules for Buildings, 2004. ⟨www.saiglobal.com/shop⟩.
[16] ACI 318, American Concrete Institute, ACI Building Code Requirements for Reinforced Concrete, ACI 318-08, 2008.
[17] J. Schlumpf, Self-compacting concrete structures in Switzerland, Tunn. Undergr. Space Technol. 19 (2004) 480, https://doi.org/10.1016/j.tust.2004.02.080.
[18] D. Bonen, S.P. Shah. The Effects of Formulation on the Properties of Self-consolidating Concrete, 2005, pp. 43–56, https://doi.org/10.1617/2912143586.005.
[19] Z. Hashin, S. Shtrikman, A variational approach to the theory of the elastic behaviour of multiphase materials, J. Mech. Phys. Solids 11 (1963) 127–140, https://doi.org/10.1016/0022-5096(63)90060-7.
[20] R. Hill, The elastic behaviour of a crystalline aggregate, Proc. Phys. Soc. Sect. A 65 (1952) 349–354, https://doi.org/10.1088/0370-1298/65/5/307.
[21] J.D. Eshelby, The determination of the elastic field of an ellipsoidal inclusion in an anisotronic medium, Proc. R. Soc. Lond. Ser. A Math. Phys. Sci. 241 (1957) 376–396.
[22] T. Mori, K. Tanaka, Average stress in matrix and average elastic energy of materials with misfitting inclusions, Acta Met. 21 (1973) 571–574.
[23] S. Nemat-Nasser, H. Hori, Micromechanics: Overall Properties of Heterogeneous Materials, Elsevier Science, 1993, https://doi.org/10.1007/BF00437113.
[24] R.M. Christensen, K.N. Lo, Solutions for effective shear properties, J. Mech. Phys. Solids 27 (1979) 315–330.
[25] R. Hill, A self-consistent mechanics of composite materials, J. Mech. Phys. Solids 13 (1965) 213–222, https://doi.org/10.1016/0022-5096(65)90010-4.
[26] A. Qsymah, R. Sharma, Z. Yang, L. Margetts, P. Mummery, Micro X-ray computed tomography image-based two-scale homogenisation of ultra high performance fibre reinforced concrete, Constr. Build. Mater. 130 (2017) 230–240, https://doi.org/10.1016/j.conbuildmat.2016.09.020.
[27] W. Ogierman, G. Kokot, Homogenization of inelastic composites with misaligned inclusions by using the optimal pseudo-grain discretization, Int. J. Solids Struct. 113–114 (2017) 230–240, https://doi.org/10.1016/j.ijsolstr.2017.03.008.
[28] O. Pierard, C. González, J. Segurado, J. LLorca, I. Doghri, Micromechanics of elasto-plastic materials reinforced with ellipsoidal inclusions, Int. J. Solids Struct. 44 (2007) 6945–6962, https://doi.org/10.1016/j.ijsolstr.2007.03.019.
[29] D. Stefaniuk, P. Niewiadomski, M. Musiał, D. Łydżba, Elastic properties of self-compacting concrete modified with nanoparticles: multiscale approach, Arch. Civ. Mech. Eng. 19 (2019) 1150–1162, https://doi.org/10.1016/j.acme.2019.06.006.
[30] C.F. Dunant, B. Bary, A.B. Giorla, C. Péniguel, J. Sanahuja, C. Toulemonde, A.B. Tran, F. Willot, J. Yvonnet, A critical comparison of several numerical methods for computing effective properties of highly heterogeneous materials, Adv. Eng. Softw. 58 (2013) 1–12, https://doi.org/10.1016/j.advengsoft.2012.12.002.
[31] I.M. Gitman, H. Askes, L.J. Sluys, Representative volume: existence and size determination, Eng. Fract. Mech. 74 (2007) 2518–2534, https://doi.org/10.1016/j.engfracmech.2006.12.021.
[32] E. Gal, R. Kryvoruk, Meso-scale analysis of FRC using a two-step homogenization approach, Comput. Struct. 89 (2011) 921–929, https://doi.org/10.1016/j.compstruc.2011.02.006.
[33] E.J. Garboczi, J.G. Berryman, Elastic moduli of a material containing composite inclusions: effective medium theory and finite element computations, Mech. Mater. 33 (2001) 455–470, https://doi.org/10.1016/S0167-6636(01)00067-9.
[34] J.C. Nadeau, A multiscale model for effective moduli of concrete incorporating ITZ water-cement ratio gradients, aggregate size distributions, and entrapped voids, Cem. Concr. Res. 33 (2003) 103–113, https://doi.org/10.1016/S0008-8846(02)00931-6.
[35] K.Y. Kim, T.S. Yun, J. Choo, D.H. Kang, H.S. Shin, Determination of air-void parameters of hardened cement-based materials using X-ray computed tomography, Constr. Build. Mater. 37 (2012) 93–101, https://doi.org/10.1016/j.conbuildmat.2012.07.012.
[36] R.C.K. Wong, K.T. Chau, Estimation of air void and aggregate spatial distributions in concrete under uniaxial compression using computer tomography scanning, Cem. Concr. Res. 35 (2005) 1566–1576, https://doi.org/10.1016/j.cemconres.2004.08.016.

[37] T. Ponikiewski, J. Katzer, M. Bugdol, M. Rudzki, Determination of 3D porosity in steel fibre reinforced SCC beams using X-ray computed tomography, Constr. Build. Mater. 68 (2014) 333–340, https://doi.org/10.1016/j.conbuildmat.2014.06.064.
[38] C. Bao, J.H. Bi, D. Xu, J. Guan, W.X. Cheng, Numerical simulation of the distribution and orientation of steel fibres in SCC, Mag. Concr. Res. 72 (2020) 1102–1111, https://doi.org/10.1680/jmacr.18.00432.
[39] M.S. Abo Dhaheer, M.M. Al-Rubaye, W.S. Alyhya, B.L. Karihaloo, S. Kulasegaram, Proportioning of self–compacting concrete mixes based on target plastic viscosity and compressive strength: part I - mix design procedure, J. Sustain Cem. Mater. 5 (2016) 199–216, https://doi.org/10.1080/21650373.2015.1039625.
[40] R. Deeb, B.L. Karihaloo, Mix proportioning of self-compacting normal and high-strength concretes, Mag. Concr. Res. 65 (2013) 546–556, https://doi.org/10.1680/macr.12.00164.
[41] EFNARC, The European Guidelines for Self-Compacting Concrete, UK, 2005. ⟨www.efnarc.org⟩.
[42] BS EN 12390-3, Testing Hardened Concrete: Compressive Strength of Test Specimens, 2009.
[43] BS EN 12390-13, Determination of Secant Modulus of Elasticity in Compression, 2013.
[44] J. Yu, B. Zhang, W. Chen, J. He, Experimental and multi-scale numerical investigation of ultra-high performance fiber reinforced concrete (UHPFRC) with different coarse aggregate content and fiber volume fraction, Constr. Build. Mater. 260 (2020), 120444, https://doi.org/10.1016/j.conbuildmat.2020.120444.
[45] X. Sun, Z. Gao, P. Cao, C. Zhou, Mechanical properties tests and multiscale numerical simulations for basalt fiber reinforced concrete, Constr. Build. Mater. 202 (2019) 58–72, https://doi.org/10.1016/j.conbuildmat.2019.01.018.
[46] Y. Benveniste, A new approach to the application of Mori-Tanaka's theory in composite materials, Mech. Mater. (1987) 147–157.
[47] I. Doghri, A. Ouaar, Homogenization of two-phase elasto-plastic composite materials and structures study of tangent operators, cyclic plasticity and numerical algorithms, Int. J. Solids Struct. 40 (2003) 1681–1712, https://doi.org/10.1016/S0020-7683(03)00013-1.
[48] T. Li, W. Bai, K. Zhang, Z. Pan, A study on image-processing based identification of aspect ratio of coarse aggregate, MATEC Web Conf. 275 (2019) 02007, https://doi.org/10.1051/matecconf/201927502007.
[49] A.F. Stock, D.J. Hannant, R.I.T. Williams, D.W. Hobbs, The effect of aggregate concentration upon the strength and modulus of elasticity of concrete, Mag. Concr. Res. 32 (1980) 246–250, https://doi.org/10.1680/macr.1980.32.113.246.
[50] R. Sharma, P. Mahajan, R.K. Mittal, Elastic modulus of 3D carbon/carbon composite using image-based finite element simulations and experiments, Compos Struct. 98 (2013) 69–78, https://doi.org/10.1016/j.compstruct.2012.11.019.
[51] L. Shuguang, L. Qingbin, Method of meshing ITZ structure in 3D meso-level finite element analysis for concrete, Finite Elem. Anal. Des. 93 (2015) 96–106, https://doi.org/10.1016/j.finel.2014.09.006.
[52] J. Liu, C. Li, J. Liu, G. Cui, Z. Yang, Study on 3D spatial distribution of steel fibers in fiber reinforced cementitious composites through micro-CT technique, Constr. Build. Mater. 48 (2013) 656–661, https://doi.org/10.1016/j.conbuildmat.2013.07.052.
[53] X. Qin, Q. Xu, Statistical analysis of initial defects between concrete layers of dam using X-ray computed tomography, Constr. Build. Mater. 125 (2016) 1101–1113, https://doi.org/10.1016/j.conbuildmat.2016.08.149.
[54] L. Sorelli, G. Constantinides, F.J. Ulm, F. Toutlemonde, The nano-mechanical signature of ultra high performance concrete by statistical nanoindentation techniques, Cem. Concr. Res. 38 (2008) 1447–1456, https://doi.org/10.1016/j.cemconres.2008.09.002.
[55] A. Leemann, B. Münch, P. Gasser, L. Holzer, Influence of compaction on the interfacial transition zone and the permeability of concrete, Cem. Concr. Res. 36 (2006) 1425–1433, https://doi.org/10.1016/j.cemconres.2006.02.010.
[56] E.P. Koehler, D.W. Fowler, Aggregates in Self-Consolidating Concrete, The Aggregates Foundation for Technology, Research and Education, Research Report ICAR, Austin, TX, 2007.
[57] S. Pavía, E. Condren, Study of the durability of OPC versus GGBS concrete on exposure to silage effluent, J. Mater. Civ. Eng. 20 (2008) 313–320, https://doi.org/10.1061/(asce)0899-1561(2008)20:4(313).
[58] V. Limbachiya, E. Ganjian, P. Claisse, Strength, durability and leaching properties of concrete paving blocks incorporating GGBS and SF, Constr. Build. Mater. 113 (2016) 273–279, https://doi.org/10.1016/j.conbuildmat.2016.02.152.
[59] E. Jasiūnienė, V. Cicėnas, P. Grigaliūnas, Ž. Rudžionis, A.A. Navickas, Influence of the rheological properties on the steel fibre distribution and orientation in self-compacting concrete, Mater. Struct. Mater. Constr. 51 (2018), https://doi.org/10.1617/s11527-018-1231-y.
[60] S. Zhang, L. Liao, S. Song, C. Zhang, Experimental and analytical study of the fibre distribution in SFRC: a comparison between image processing and the inductive test, Compos. Struct. 188 (2018) 78–88, https://doi.org/10.1016/j.compstruct.2018.01.006.